Electronic Supplementary Material (ESI) for Journal of Materials Chemistry C.
This journal is © The Royal Society of Chemistry 2020

Electronic Supplementary Information

A lanthanide coordination polymer as a ratiometric fluorescent probe for rapid and visual sensing of phosphate based on the target-triggered competitive effect

Lei Han, Shi Gang Liu, Yu Zhu Yang, Yu Zhu Fan, Jiao Zhou, Xing Yue Zhang, Nian Bing Li, * and Hong Qun Luo*

Key Laboratory of Eco-environments in Three Gorges Reservoir Region (Ministry of Education), School of Chemistry and Chemical Engineering, Southwest University, Chongqing 400715, P. R. China

*Corresponding Authors

*Nian Bing Li and Hong Qun Luo

*Tiansheng Road, BeiBei District, Chongqing, 400715, P. R. China. Tel: +86 23 68253237; fax: +86 23 68253237; E-mail address: linb@swu.edu.cn; luohq@swu.edu.cn

Table of Contents

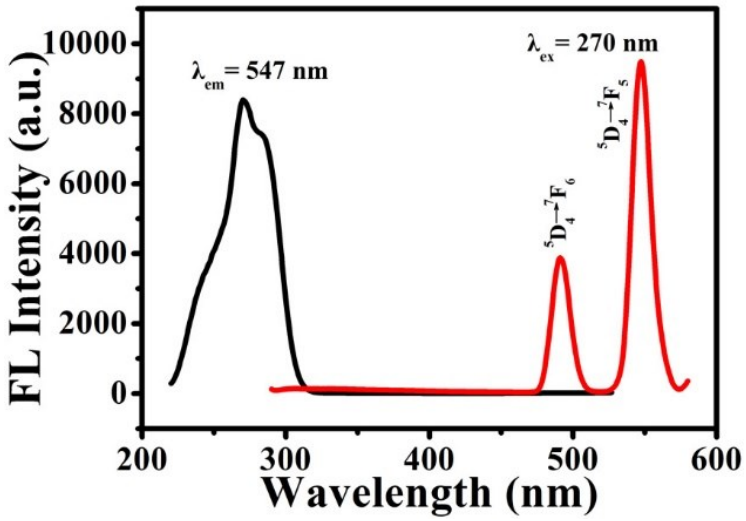

Fig. S1 Fluorescence spectra of TbGMP. Experimental conditions: 100 mM HEPES buffer, pH 7.2; Tb^{3+}, 250 μM; GMP, 200 μM.

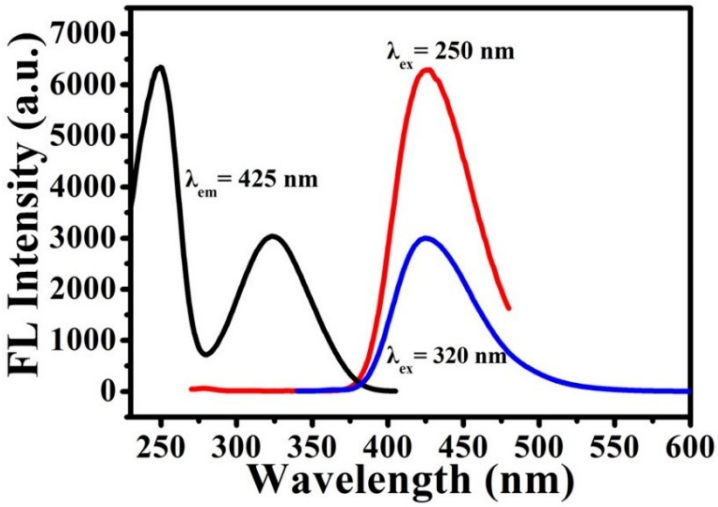

Fig. S2 Fluorescence spectra of NH_2-BDC. Experimental conditions: 100 mM HEPES buffer, pH 7.2; NH_2-BDC, 1.5 μM.

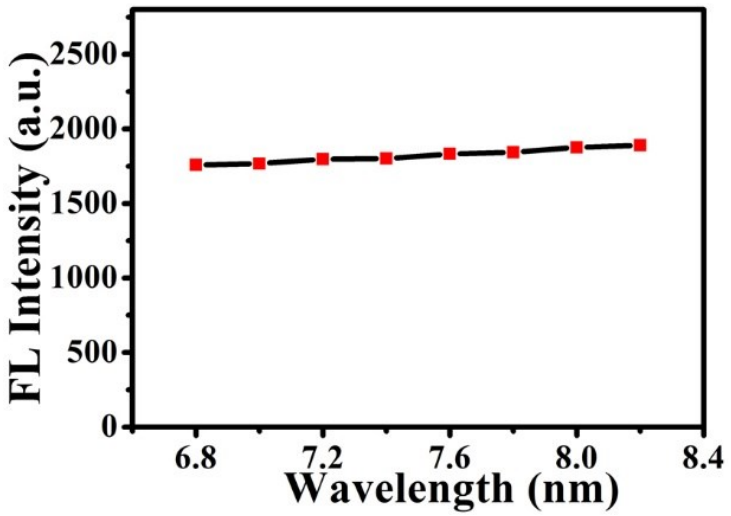

Fig. S3 Effect of pH on the fluorescence intensity of NH_2-BDC. Experimental conditions: 100 mM HEPES buffer with various pH values; NH_2-BDC, 1.5 μM; λ_{ex} = 300 nm; λ_{em} = 425 nm.

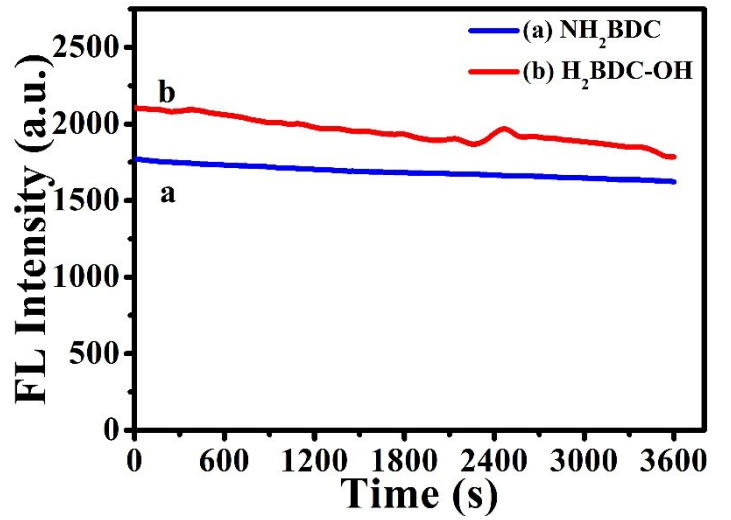

Fig. S4 Fluorescence intensity change of NH_2-BDC (a) and H_2-BDC-OH (b) under the Xe light with a photomultiplier tube voltage of 400 V continuous radiation. Experimental conditions: 100 mM HEPES buffer, pH 7.2; NH_2-BDC, 1.5 μM; H_2-BDC-OH, 1.5 μM; λ_{ex} = 300 nm; λ_{em} = 425 nm.

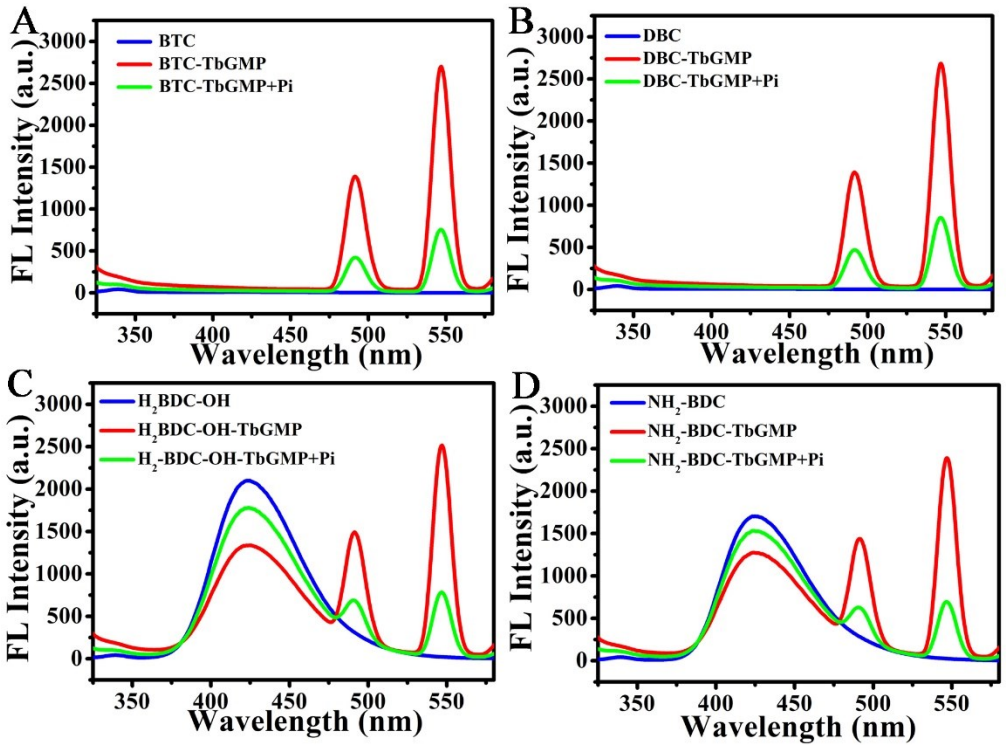

Fig. S5 Comparison of some common ligands for ratiometric sensing of Pi. (A) 1, 3, 5-Benzenetricarboxylic acid (BTC), (B) 3, 5-dicarboxylicphenyl boric acid (DBC), (C) 2-hydroxyterephthalic acid (H_2BDC-OH), and (D) NH_2-BDC served as the ligand for ratiometric sensing of Pi. Experimental conditions: 100 mM HEPES buffer, pH 7.2; BTC, 1.5 μM; DBC, 1.5 μM; H_2BDC-OH, 1.5 μM; NH_2-BDC, 1.5 μM; Tb^{3+}, 250 μM; GMP, 200 μM; Pi, 100 μM; λ_{ex} = 300 nm.

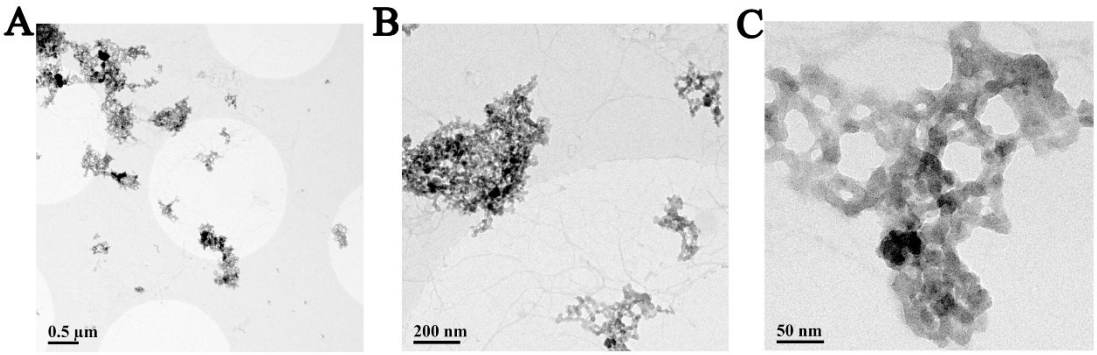

Fig. S6 TEM images of NH_2-BDC–TbGMP CPs at different magnifications.

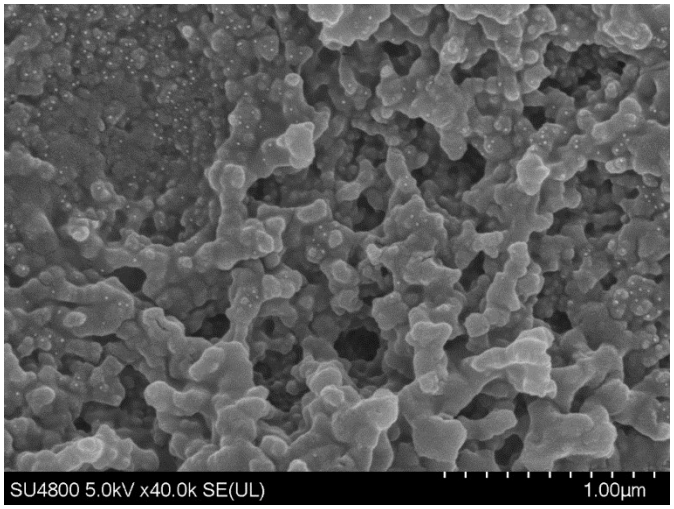

Fig. S7 SEM image of NH_2-BDC-TbGMP CPs.

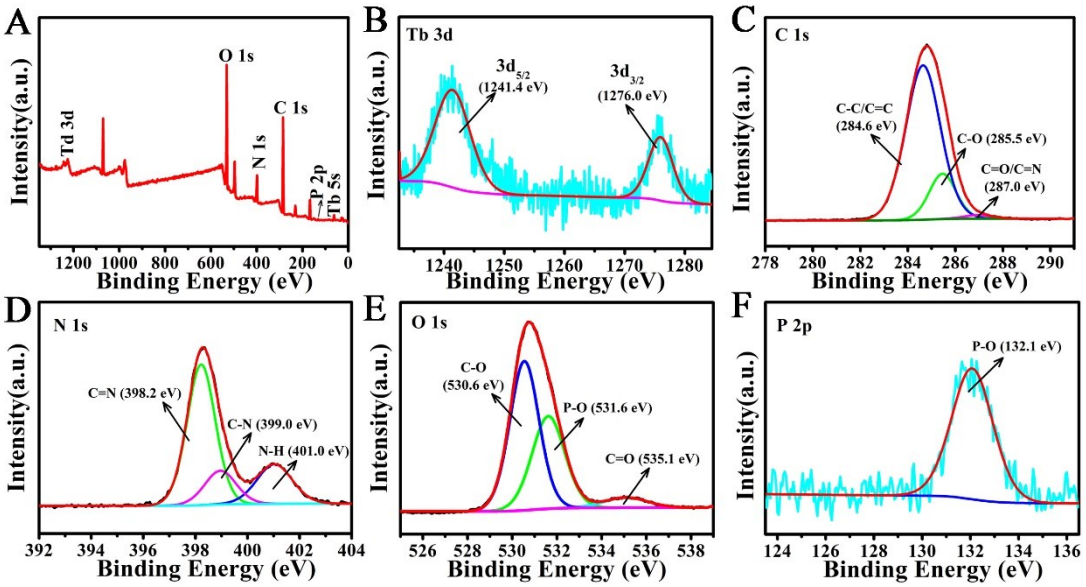

Fig. S8 (A) XPS full spectrum of NH_2-BDC–TbGMP CPs. Fitted high-resolution XPS spectra of NH_2-BDC–TbGMP CPs for (B) Tb 3d, (C) C 1s, (D) N 1s, (E) O 1s, and (F) P 2p.

Table S1 Fluorescence lifetimes of NH_2-BDC in different systems (λ_{em} = 425 nm).

System	τ (ns)
NH_2-BDC	15.32
NH_2-BDC–Tb^{3+}	15.00
NH_2-BDC–TbGMP	15.14
NH_2-BDC–TbGMP+Pi	15.03

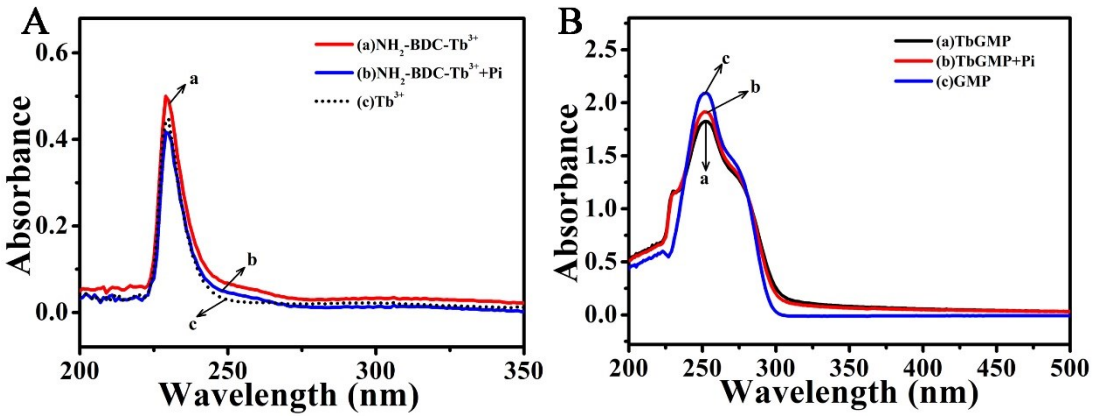

Fig. S9 (A) UV–vis absorption spectra of NH_2-BDC–Tb^{3+} (a), NH_2-BDC–Tb^{3+} + Pi (b), and Tb^{3+} (c). (B) UV–vis absorption spectra of TbGMP (a), TbGMP + Pi (b), and GMP (c). Experimental conditions: 100 mM HEPES buffer, pH 7.2; NH_2-BDC, 1.5 μM; Tb^{3+}, 250 μM; GMP, 200 μM; Pi, 100 μM.

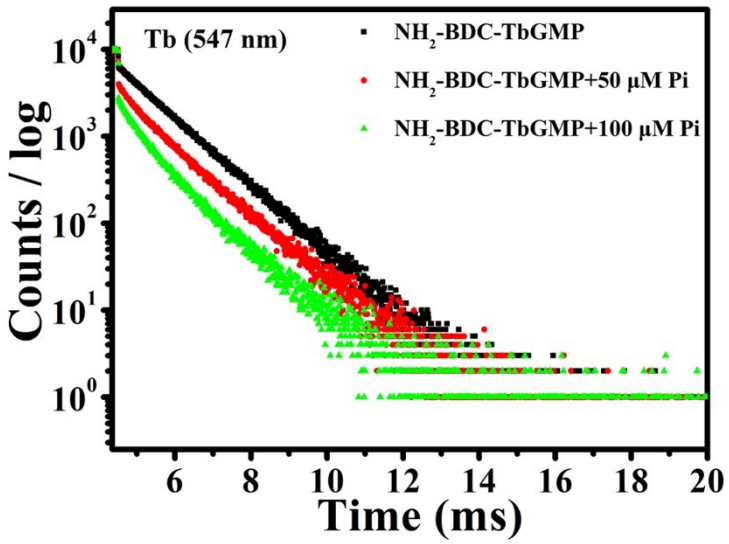

Fig. S10 Fluorescence decay (λ_{em} = 547 nm) curves of NH_2-BDC–TbGMP CPs ratiometric fluorescent probe after the addition of different concentrations of Pi.

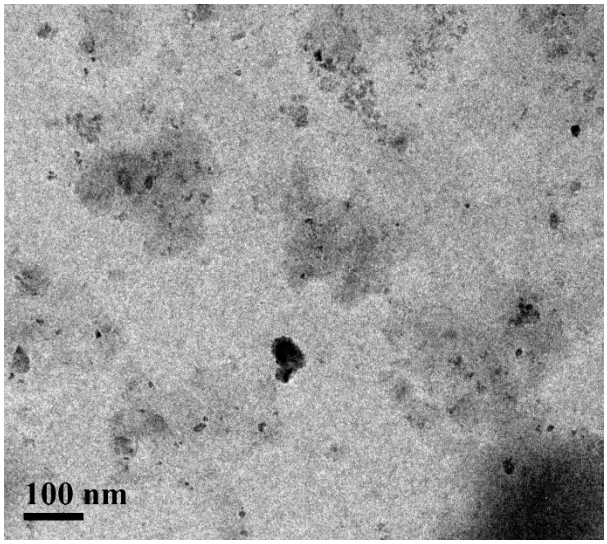

Fig. S11 TEM image of NH_2-BDC–TbGMP CPs after the reaction with Pi.

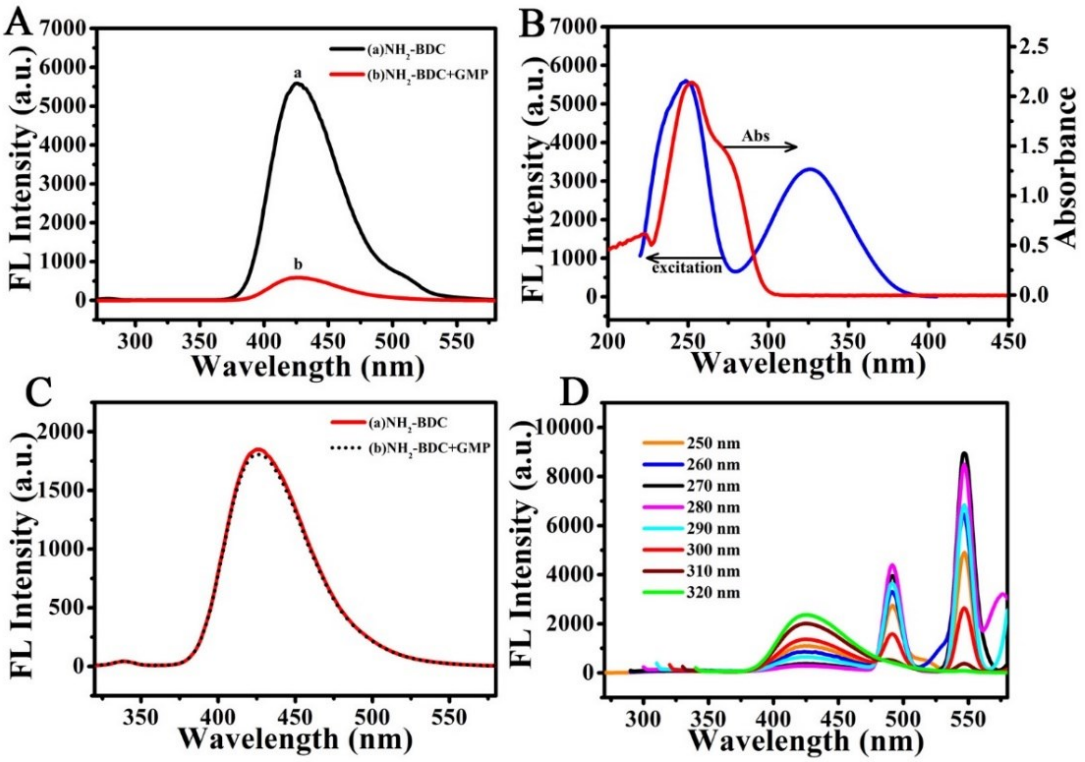

Fig. S12 (A) Fluorescence emission spectra of NH_2-BDC before and after the addition of GMP (λ_{ex} = 250 nm). (B) Fluorescence excitation spectrum of NH_2-BDC and UV–vis absorption spectrum of GMP. (C) Fluorescence emission spectra of NH_2-BDC before and after the addition of GMP (λ_{ex} = 300 nm). (D) Fluorescence emission spectra of NH_2-BDC–TbGMP CPs under different excitation wavelengths. Experimental conditions: 100 mM HEPES buffer, pH 7.2; NH_2-BDC, 1.5 μM; Tb^{3+}, 250 μM; GMP, 200 μM.

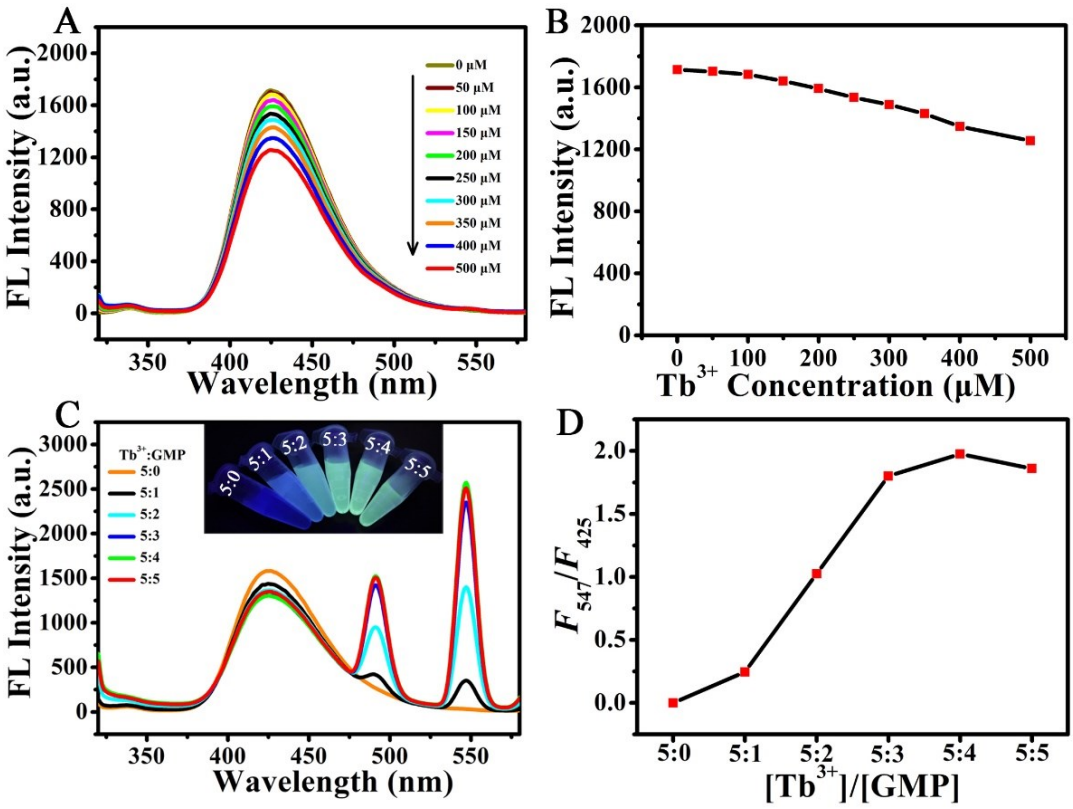

Fig. S13 Fluorescence spectra (A) and intensities change (B) of NH_2-BDC in the presence of different concentrations of Tb^{3+}. Fluorescence spectra (C) and fluorescence intensity ratio (F_{547}/F_{425}) (D) of NH_2-BDC–Tb^{3+} complexes after the addition of different concentrations of GMP (A). The inset of Figure C shows the corresponding images under a 254 nm UV lamp. Experimental conditions: 100 mM HEPES buffer, pH 7.2; NH_2-BDC, 1.5 μM; λ_{ex} = 300 nm.

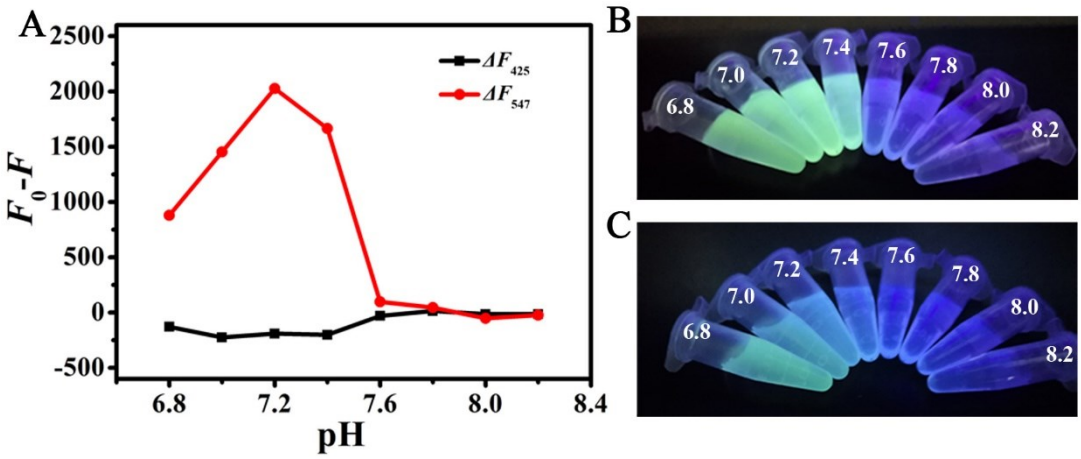

Fig. S14 Effect of pH on the fluorescence response of the sensing system for Pi detection (A). F_0 and F denote the fluorescence intensity of the sensing system before and after the addition of Pi, respectively. The corresponding images of the sensing system before (B) and after (C) the addition of Pi. Experimental conditions: 100 mM HEPES buffer with various pH; NH_2-BDC, 1.5 μM; Tb^{3+}, 250 μM; GMP, 200 μM; Pi, 100 μM; λ_{ex} = 300 nm.

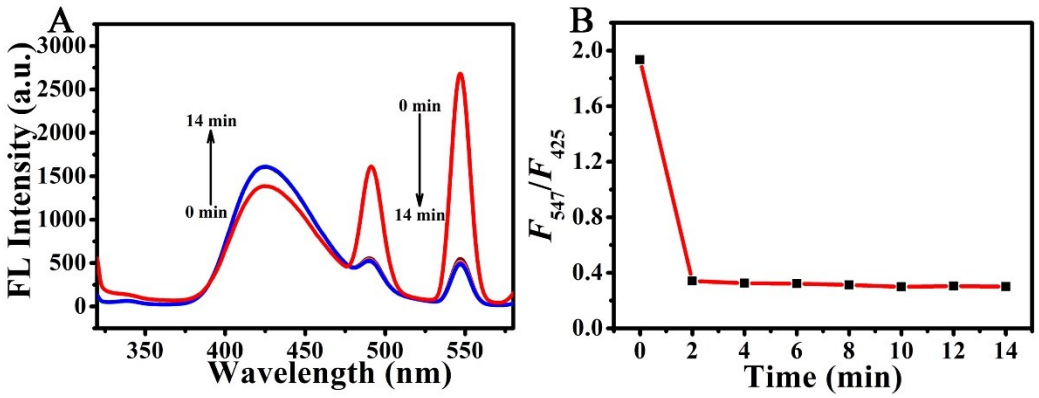

Fig. S15 Fluorescence spectra (A) and fluorescence intensity ratio (F_{547}/F_{425}) (B) of NH_2-BDC–TbGMP CPs versus reaction time in the presence of Pi. Experimental conditions: 100 mM HEPES buffer, pH 7.2; NH_2-BDC, 1.5 μM; Tb^{3+}, 250 μM; GMP, 200 μM; Pi, 100 μM; λ_{ex} = 300 nm.

Table S2 Comparison of some reported approaches for Pi detection.

Method	Sensing system	Detection time (min)	Linear range (μM)	LOD (μM)	Ref.
Colorimetry	Au NP [a]	15	0.5–30	0.076	1
Colorimetry	PCN-222 NR [b]	240	0.25–25	0.22	2
Electrochemistry	MoP [c]	60	100–20000	30	3
Electrochemistry	Paper electrode	2.5	10–300	4	4
Fluorescence	Eu-MOF [d]	40	0.1–15	0.052	5
Fluorescence	CDs [e]–Al^{3+}	5	0.25–7.5	0.1	6
Fluorescence	CIP [f] –Eu^{3+}	10	0.02–4.0	0.0043	7
Fluorescence	Cu NCs [g]–Eu^{3+}	5	0.07–80	0.0096	8
Fluorescence	GQDs [h]–Eu^{3+}	10	0.5–190	0.1	9
Fluorescence	GQDs–$Mo_7O_{24}^{6-}$ [i]	0.5	7–30	0.05	10
Fluorescence	Mn-ZnS QDs–Ce^{3+} [j]	5	8–320	2.71	11
Fluorescence	Au NCs–Eu^{3+}	15	0.5–200	0.18	12
Fluorescence	uranine@ZIF-8 [k]	3	1–500	0.2	13
Fluorescence	Eu@BUC-14 [l]	5	5–150	0.88	14
Fluorescence	Zr-MOF@rhodamine B	120	80–400	2	15
Fluorescence	Zr-MOFs	90	5–150	1.25	16
Fluorescence	NH_2-BDC–TbGMP	2	0.5–100	0.13	This work

[a] Au NP: gold nanoparticles; [b] PCN-222 NR: porphyrinic metal−organic framework nanorod;
[c] MoP: molybdenum phosphide modified electrode; [d] MOF: metal-organic frameworks;
[e] CDs: carbon dots; [f] CIP: Ciprofloxacin; [g] NCs: nanoclusters; [h] GQDs: graphene quantum dots;
[i] $Mo_7O_{24}^{6-}$: molybdate; [j] QDs: quantum dots; [k] ZIF-8: zeolitic imidazolate framework-8;
[l] Eu@BUC-14: lanthanide functionalized coordination polymers.

Table S3 The CIE coordinates value of the ratiometric fluorescent sensor for various concentrations of Pi.

Pi (μM)	CIE x	CIE y
0	0.1845	0.2663
0.5	0.1841	0.2635
1	0.1841	0.2634
2	0.1839	0.2616
5	0.1833	0.2575
20	0.1812	0.2426
40	0.1762	0.2070
60	0.1711	0.1711
80	0.1680	0.1486
100	0.1637	0.1170

Table S4 The CIE coordinates value of the ratiometric fluorescent sensor for different anions.

Anions	CIE x	CIE y
Blank	0.1843	0.2641
F^-	0.1831	0.2556
Cl^-	0.1830	0.2552
Br^-	0.1832	0.2560
I^-	0.1828	0.2540
NO_3^-	0.1834	0.2580
Ac^-	0.1828	0.2538
HCO_3^-	0.1827	0.2533
CO_3^{2-}	0.1834	0.2579
SO_3^{2-}	0.1841	0.2628
SO_4^{2-}	0.1831	0.2561
S^{2-}	0.1831	0.2558
SCN^-	0.1834	0.2577
Pi	0.1631	0.1130

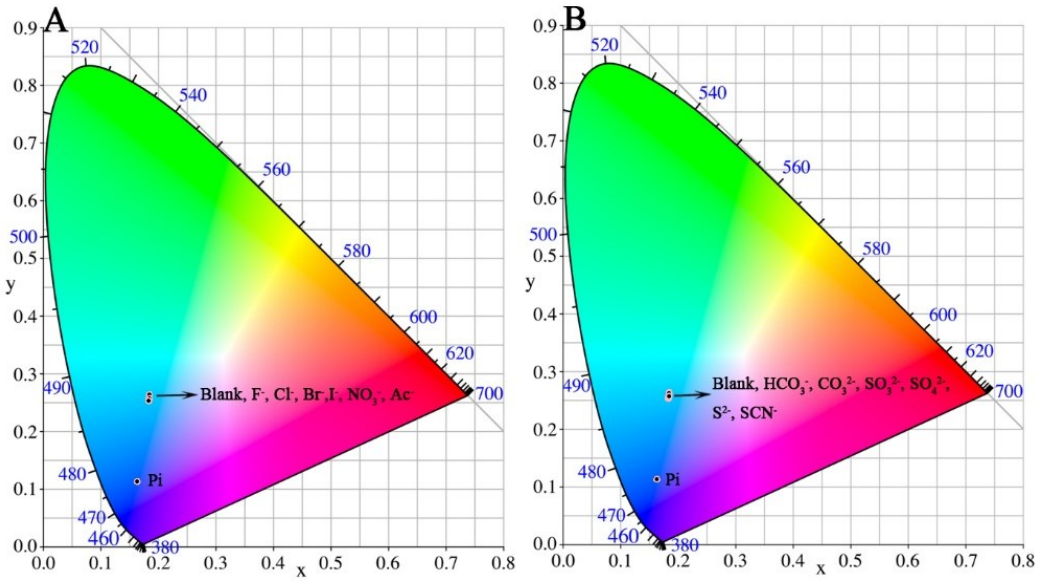

Fig. S16 CIE chromaticity coordinates of the sensing system for different anions.

Table S5 Detection results of Pi in the real water samples (n = 3).

Sample	Added (μM)	Found [a] (μM)	Recovery (%)	RSD(%)
	0	3.82	—	5.76
river water	10	14.89	110.7	5.50
	30	37.50	112.3	1.44

[a] The mean of three measurements.

References

1 W. Q. Liu, Z. F. Du, Y. Qian and F. Li, *Sens. Actuators B Chem*., 2013, **176**, 927–931.

2 C. M. Cheng, R. L. Zhang, J. H. Wang, Y. Zhang, S. S. Xiong, Y. Huang and M. Yang, *ACS Appl. Mater. Interfaces*, 2020, **12**, 26391–26398.

3 J. X. Zhang, Y. X. Bian, D. Liu, Z. W. Zhu, Y. H. Shao and M. X. Li, *Anal. Chem*., 2019, **91**, 14666−14671.

4 S. Cinti, D. Talarico, G. Palleschi, D. Moscone and F. Arduini, *Anal. Chim. Acta*, 2016, **919**, 78−84.

5 Y. Cheng, H. M. Zhang, B. Yang, J. Wu, Y. X. Wang, B. Ding, J. Z. Huo and Y. Li, *Dalton Trans.*, 2018, **47**, 12273–12283.

6 B. B. Chen, R. S. Li, M. L. Liu, H. Y. Zou, H. Liu and C. Z. Huang, *Talanta,* 2018, **178**, 172–177.

7 H. F. Wu and C. L. Tong, *ACS Sens.,* 2018, **3**, 1539–1545.

8 H. Y. Cao, Z. H. Chen and Y. M. Huang, *Talanta,* 2015, **143**, 450–456.

9 J. M. Bai, L. Zhang, R. P. Liang and J. D. Qiu, *Chem. Eur. J.*, 2013, **19** 3822–3826.

10 Y. H. Wang, W. Y. Weng, H. Xu, Y. Luo, D. Guo, D. Li and D. W. Li, *Anal. Chim. Acta,* 2019, **1080** 196–205.

11 J. Qin, D. X. Li, Y. M. Miao and G. Q. Yan, *RSC Adv.*, 2017, **7**, 46657−46664.

12 S. N. Ding, C. M. Li, B. H. Gao, O. Kargbo, N. Wan, X. Chen and C. Zhou, *Microchim. Acta,* 2014, **181**, 1957–1963.

13 H. H. Li, F. X. Fu, W. T. Yang, L. Ding, J. X. Dong, Y. Yang, F. X. Wang and Q. H. Pan, *Sens. Actuators B Chem.*, 2019, **301**, 127110.

14 Y. Q. Zhang, S. S. Sheng, S. Mao, X. H. Wu, Z. Li, W. Q. Tao and I. R. Jenkinson, *Water Res.*, 2019, **163**, 114883.

15 N. Gao, J. Huang, L. Y. Wang, J. Y. Feng, P. C. Huang and F. Y. Wu, *Appl. Surf. Sci.*, 2018, **459**, 686−692.

16 J. Yang, Y. Dai, X. Y. Zhu, Z. Wang, Y. S. Li, Q. X. Zhuang, J. L. Shi and J. L.

Gu, *J. Mater. Chem. A,* 2015, **3**, 7445–7452.